Climate
of the Past
Discussions

Interactions between the Northern-Hemisphere ice sheets and climate during the Last Glacial Cycle

Meike D. W. Scherrenberg[1], Constantijn J. Berends[1], Lennert B. Stap[1], Roderik S.W. van de Wal[1,2]

[1]Institute for Marine and Atmospheric research Utrecht, Utrecht University, 3584 CC Utrecht, the Netherlands
5   [2]Faculty of Geosciences, Department of Physical Geography, Utrecht University, Utrecht, the Netherlands

Correspondence to: M.D.W. Scherrenberg (M.D.W.Scherrenberg@uu.nl)

Abstract. During the Last Glacial Cycle (LGC), ice sheets covered large parts of Eurasia and North America which resulted in ~120 meters of sea level change. Ice sheet – climate interactions have considerable influence on temperature and precipitation patterns, and therefore need to be included when simulating this time period. Ideally, ice sheet – climate

10   interactions are simulated by a high-resolution earth system model. While these models are capable of simulating climates at a certain point in time, such as the Pre-Industrial (PI) or the Last Glacial Maximum (LGM; 21,000 years ago), a full glacial cycle is currently unfeasible as it requires a too large amount of computation time. Nevertheless, ice-sheet models require forcing that captures the gradual change in climate over time to calculate the accumulation and melt of ice and its effect on ice sheet extent and volume changes.

15   Here we simulate the LGC using an ice sheet model forced by LGM and PI climates. The gradual change in climate is modelled by transiently interpolating between pre-calculated results from a climate model for the LGM and the PI. To assess the influence of ice sheet – climate interactions, we use two different interpolation methods: The climate matrix method, which includes these interactions, and the glacial index method, which does not. To investigate the sensitivity of the results to the prescribed climate forcing, we use the output of several models that are part of the

20   Paleoclimate Modelling Intercomparison Project Phase III (PMIP3). In these simulations, ice volume is prescribed and the climate is reconstructed. Here we test those models by using their climate to drive an ice sheet model over the LGC.

    We find that the differences caused by the climate forcing exceeds the differences caused by the interpolation method. Some General Circulation Models (GCMs) produced unrealistic LGM volumes and only four resulted in reasonable ice sheets with LGM Northern Hemisphere sea level contribution ranging between 74 – 113 meters with

25   respect to the present day. The glacial index and climate matrix methods result in similar ice volumes at LGM but yield a different ice evolution with different ice domes during the inception phase of the glacial cycle, and different sea-level rates during the deglaciation phase. The temperature-albedo feedback is the main cause of differences between the glacial index and climate matrix methods.

1 Introduction

30   Sea-level rise due to the melt of the Greenland and Antarctic ice sheets is one of the biggest threats posed by anthropogenic climate change (Fox-Kemper et al., 2021). Ice sheets have a substantial influence on the climate system, as these can amplify changes in temperatures and alter precipitation patterns, which in turn affect ice accumulation and ablation. Therefore, to make accurate projections of future sea level change, it is important to understand the interactions between the climate and the ice sheets. These interactions take place over multiple millennia as the ice sheets respond

35   slowly to changes in the climate (Clark et al., 1999). Observations are currently insufficient to study ice sheet – climate interaction as these only capture the changes in ice sheets in the past century. This is currently not enough to observe large changes in ice geometry to cause a substantial feedback effect to the climate system. Instead, paleo records provide information on the climate system such as atmospheric CO_2 concentrations, sea level, and ice thickness and extent, which date back millions of years. These reconstructions allow the study of considerable changes in the ice sheet and climate

40   that took place over multiple millennia. The most recent period in the Earth's history with substantial changes in ice sheet extent is the Last Glacial Cycle (LGC; 120,000 – 8,000 years ago). This period is associated with a sea level change of approximately 120 meters (e.g., Simms et al., 2019, Gowan et al., 2021) and a change in global temperature of 3 – 5 K (Annan & Hargreaves, 2013) with respect to present day.

        The climate during the LGC is affected by several internal and external processes in the climate system. Over

45   long-time scales, insolation changes due to orbital parameters are significant enough to affect climate and ice sheets (Löfverström et al., 2014). Additionally, atmospheric CO_2 concentrations changed between 190 and 280 ppm during the LGC, also acting as a forcing to the climate system. Topography and albedo changes resulting from the change in ice extent and thickness affects temperature and precipitation (e.g., Abe-Ouchi et al., 2007, Clark et al., 1999). Especially the temperature-albedo and precipitation-topography interactions induced by changes in ice volume were shown to have

50   a substantial impact on ice sheets (Abe-Ouchi et al., 2007, Stap et al. 2014). A decrease (increase) in temperature can prompt an increase (decrease) in snow coverage and consequentially albedo. An increase (decrease) in albedo has a net effect on the total thermal energy stored in the climate system, as a larger (smaller) portion of solar radiation entering the atmosphere is reflected towards space. Therefore, albedo can alter temperature on regional and global spatial scales. Hence, an initial decrease in temperature can lead to further cooling. Local temperatures are also affected by changes in

55   surface topography due to the atmospheric temperature lapse rate.

        Topography has a local and regional impact on precipitation. Precipitation is enhanced on the slopes of ice margins, since cooling and condensation takes place when air is moved up slopes. During this transport, air cools and moisture is removed resulting in low precipitation on the lee side and on ice plateaus. Changes in surface topography during glacial cycles can affect atmospheric circulation, again affecting temperature and precipitation patterns (Pausata

Climate
of the Past
Discussions

60 et al., 2011, Ullman et al., 2014). These feedbacks, which act over multiple millennia as the ice sheet gradually incepts, grows, and retreats, must be accounted for during transient climate and ice sheet simulations.

An ideal set-up to transiently simulate ice-sheet climate interactions during the LGC would involve a fully coupled General Circulation Model (GCM) that simulates ice sheets, oceans and atmosphere. However, these simulations require a large amount of computation time, making them currently unfeasible. One strategy to deal with this excessive

65 computational demand is to decrease grid resolution or use asynchronous coupling while certain physical processes are artificially accelerated (e.g., Smith & Gregory, 2012, Ganopolski et al., 2010). Alternatively, for specific time slices, such as the Last Glacial Maximum (LGM; 21,000 years ago) and Pre-Industrial (PI), GCMs can be used. Modelling efforts such as the Paleoclimate Modelling Intercomparison Project (PMIP) intercompare a set of GCMs that used similar boundary conditions, such as atmospheric CO_2 concentration, orbital configuration, and fixed prescribed ice-sheet

70 geometry, to simulate the climate for a specific time slice. The third phase of PMIP, PMIP3 (Braconnot et al., 2011), used nine GCMs to simulate climates during LGM and PI. Each climate model used prescribed ice sheets by Abe Ouchi et al. (2015), hence transient changes in ice topography were not simulated. Despite using the same boundary conditions, ice-sheet model studies using the PMIP3 models such as Niu et al., (2019) and Alder & Hostetler, (2019) found substantial differences in LGM ice volume and extent. In these studies, Niu simulated the entire last glacial cycle while

75 Adeler & Hostetler used steady state LGM climate forcing, both finding large differences between the ice sheets resulting from the GCM climates, some showing unrealistic ice sheets.

Simulating a full glacial cycle using an ice-sheet model is feasible as these require only a small amount of run-time compared to GCMs. GCMs model the entire globe and simulate processes that require small time steps. Ice-sheet models can run at a much lower temporal resolution and only require a grid that covers a small portion of the Earth, but

80 they need a higher spatial resolution. However, ice-sheet models can require information on the evolution of temperature and precipitation to calculate melt and accumulation of ice sheets.

In the past different methods have been used to include transiently changing climate forcing to an ice-sheet model. The LGC has been forced by applying a temperature anomaly (De Boer, 2014), coupling the ice-sheet to a simple climate model (Stap et al., 2014), or by using a glacial index method (Niu et al., 2019). In the glacial index method LGM

85 and PI temperature and precipitation are transiently interpolated with respect to one parameter obtained from paleo-reconstructions, such as CO_2. Therefore, as CO_2 decreases, the climate cools and dries as it approaches LGM. This method has been shown to yield LGM ice volume and extent that agrees well with reconstructions (e.g, Charbit et al., 2007, Niu et al., 2019). However, this interpolation does not include any ice sheet – climate interactions. To parameterize these feedbacks, we can use a climate matrix method instead (Pollard., 2010). The climate matrix method implicitly

90 resolves the temperature-albedo and precipitation-topography feedbacks. Here, the climate time slices are interpolated with respect to both prescribed forcing, for example atmospheric CO_2 concentrations, and the internally calculated albedo

and ice sheet geometry. Since it incorporates calculated fields from the ice sheet model into the interpolation, a climate matrix method can implicitly resolve ice sheet – climate feedbacks requiring only a small amount of additional computational resources. When performing realistic scenarios of the LGC, the climate matrix method was shown to be

95 able to successfully replicate ice evolution (Berends et al., 2018).

While the climate matrix method and glacial index method have been used in the past, a comparison with a realistic scenario for the LGC has not yet been explored. Recently, Stap et al. (2022) compared a matrix and index method with schematic experiments of Antarctica during the Miocene. This showed that the temperature-albedo and precipitation-topography feedback work in opposite ways: The temperature-albedo feedback substantially reduces, and

100 precipitation-topography feedback slightly increases glacial-interglacial variability. They suggested that the temperature-albedo feedback is stronger than the precipitation-topography feedback.

Here we aim to build upon the work by Stap et al. (2022) by intercomparing a glacial index and climate matrix method using a realistic experiment by simulating the Northern Hemisphere ice sheets during LGC. We force the ice-sheet model using different available climate model output from the PMIP3 ensemble. This study uses a climate matrix

105 method, therefore also building on Niu et al., 2019, who simulated the LGC using PMIP3 climate forcing interpolated with a glacial index method. Our ice-sheet model and climate forcing set-up are described in section 2. Section 3 introduces our simulations of the LGC and shows the differences due to climate forcing and due to the interpolation methods. These findings are discussed in section 4.

2. Methods

110 In this section, we introduce the ice-sheet model and climate forcing that were used to simulate the LGC. First, we describe IMAU-ICE, the ice-sheet model used in this study. Secondly, we discuss the parameterized SMB scheme that has been used to calculate accumulation and ablation. Thirdly, we introduce the temperature and precipitation climate forcing used to simulate the LGC. Lastly, the climate matrix and glacial index methods are introduced.

2.1 Ice sheet model

115 In this study, we use the three-dimensional thermodynamically-coupled ice-sheet model IMAU-ICE version 2.0 (Berends et al., 2022). This model uses the depth-integrated viscosity approximation (DIVA; Goldberg, 2011) to calculate the dynamics of floating and grounded ice. This vertically-integrated approximation to the stress balance is similar to the hybrid SIA/SSA, but has improved physics, is more efficient and has improved numerical stability (Berends et al., 2022). A regularised Coulomb sliding law is used to calculate basal friction (Bueler & van Pelt, 2015). Proper

120 grounding-line migration is achieved using a sub-grid friction-scaling scheme, which is based on the approach used in

PISM (Feldmann et al., 2014) and CISM (Leguy et al., 2021). Sub-shelf melt rates are calculated using a temperature and depth-dependent sub-shelf melt parameterization (Martin et al. 2011) in combination with parameterised ocean temperatures (De Boer et al., 2013). Bedrock adjustment to changes in ice load is modelled using the ELRA (Elastic Lithosphere, Relaxing Asthenosphere) model (Le Meur and Huybrechts, 1996). Calving is not included in this version

125 of the model.

We simulate the North American, Eurasian and Greenland ice sheets concurrently in three separate domains with a 40x40km, 40x40km, and 20x20km resolution respectively (see Fig. 1). To prevent double counting of ice, ice growth is prevented in the Greenlandic parts of the North American and Eurasian domains and Ellesmere Island in the Greenland

130 domain. Antarctica is not included in these simulations as the feedbacks from topography and albedo throughout the LGC are small compared to Eurasia and North America, because of the relatively small changes in the ice sheet.

2.2 Surface mass balance

The monthly surface mass balance (SMB) is calculated from the monthly temperature and precipitation resulting from the climate interpolation (see 2.4) using an insolation-temperature model (IMAU-ITM; Berends et al., 2018). In this

135 parameterized SMB scheme, snow accumulation is calculated using a precipitation and temperature-dependent snow-rain partitioning by Ohmura, (1999). This snow-rain partitioning was tuned towards the regional climate model RACMO as part of the Greenland Surface Mass Balance Model Intercomparison Project (GrSMBMIP; Fettweis et al., 2020). Annual refreezing is calculated using the approach by Huybrechts and de Wolde, (1999) and Janssens and Huybrechts, (2000). Ablation is parameterised and depends on temperature, insolation and surface albedo (Bintanja et al., 2002). The

140 insolation at the top of the atmosphere is prescribed and obtained from Laskar et al. (2004). Albedo is calculated internally: First a snow-free albedo is applied, with 0.1 for ocean, 0.2 for land and 0.5 for bare ice. A firn layer is added on top which, depending on depth, can increase the albedo to a maximum of 0.85. The equations governing IMAU-ITM are presented in Appendix A.

2.3 PMIP3 climate time slices

145 We obtained climate forcing for near-surface air temperature, precipitation and topography from the nine available LGM and PI GCM simulations that are part of PMIP3. These simulations are listed in Table 1. Each of these models used boundary conditions that followed the PMIP3 protocol, such as orbital parameters, trace gases, and ice sheets. The PMIP3 protocol uses a prescribed ice sheet by Abe-Ouchi et al., 2015 which is a composite of the ICE-6G v2.0 (Argus & Peltier, 2010), GLAC-1a (Tarasov et al., 2012) and ANU (Lambeck et al., 2010). We selected a subset of the nine

150 available PMIP3 LGM and PI simulations to obtain climate forcing that result in good agreement with reconstructions,

this step is described in Appendix B. The selection consists of COSMOS, IPSL, MIROC and MPI. Our parameterized SMB scheme was tuned to the mean climate of this sub-selection, which is hereafter referred to as PMIP3-Ensemble.

To apply the GCM fields to the ice sheet model, corrections need to be applied to account for the difference in resolution and topography. First a correction is applied to deal with biases in the GCM models, which is described in

155 Appendix C. Secondly, to account for the large difference in resolution, the GCM fields are bilinearly interpolated to the ice-sheet model grid. Thirdly, since the ice-sheet model topography evolves during the LGC, which is not accounted for in the GCM climate time-slices, a topographic correction needs to be applied. Here we use the approach by Berends et al. (2018), which implies that temperature is downscaled using a dynamic lapse rate correction. Precipitation is downscaled using the Roe and Lindzen (2001) model, which accounts for surface slope, wind direction and changes in

160 surface height. Greenland experiences only small changes in topography during the LGC, so we apply a Clausius-Clapeyron relation instead, which relates changes in temperature to changes in precipitation.

2.4 Transiently changing forcing

In this study we use two methods to transiently interpolate between climate time slices: a glacial index method and a climate matrix method. In our glacial index method, precipitation and temperature fields are interpolated with respect to

165 prescribed CO_2 obtained from Bereiter et al. (2015). Fig. 2 depicts the atmospheric CO_2 concentration during the LGC and the corresponding values for the glacial index. A glacial index of 1 (0) represents full glacial (interglacial) conditions. Hence, the climate forcing is equal to LGM (PI). Temperature and precipitation are respectively interpolated linearly and logarithmically. The logarithmical interpolation for precipitation prevents negative values and is used to describe the relative changes during the LGC.

170 The climate matrix method expands upon the glacial index method by implicitly resolving the temperature-albedo and precipitation-topography feedbacks. This is achieved by making the interpolation parameter spatially variable. In this study, we applied the climate matrix method using the approach by Berends et al. (2018). Temperature is interpolated with respect to CO_2, and to the absorbed insolation at the surface. The absorbed insolation is computed using the internally calculated albedo, and the insolation solution by Laskar et al. (2004). Therefore, any modelled

175 advance (retreat) of the ice will result in an increase (decrease) in albedo, an increase (decrease) in the interpolation weight, and therefore a more glacial (interglacial) climate. Precipitation is interpolated with respect to the change in topography between LGM and PI. In the regions without ice in LGM reconstructions, precipitation is interpolated with in topography. Equations governing the glacial index and climate matrix methods are presented in Appendix D.

3. Results

180 This section introduces simulations of the LGC with a selection of PMIP3 forcing temporally interpolated using the climate matrix or glacial index method.

3.1 Climate forcing

In this section, we compare simulations of the LGC that resulted from different climate forcings using the climate matrix method. Fig. 3 shows the sea-level contribution during the LGC with the climate forcing from COSMOS, IPSL, MIROC,
185 MPI, and the PMIP3-Ensemble. The sea level contribution at LGM ranges substantially between the five simulations. As shown in Fig. 3a, the LGM sea level contribution of the Northern Hemisphere ice sheets ranges between 74 (COSMOS) and 119 (MIROC) meters of sea-level equivalent (m.s.l.e.). When including the contribution for Antarctica of 10 m.s.l.e. (Simms et al., 2019), the total LGM global sea level contribution is within range of Simms et al. for the PMIP3-Ensemble, MPI and IPSL.

190 The North American ice sheet is the largest contributor to the differences in ice volume with a LGM contribution of 56 m.s.l.e. (COSMOS) and a maximum of 87 m.s.l.e. (MIROC; Fig. 3b). For the Eurasian ice sheet, LGM sea level contribution varies between 12 m (IPSL) and 29 m (MIROC) (Fig. 3c). This substantial difference between ice sheet model runs forced by individual PMIP3-members is in line with findings by Niu et al., (2019) and Alder & Hostetler, (2019).

195 Fig. 4 shows when each region was covered by ice for the first time during the LGC, thereby indicating the timing of inception and the gradual increase in extent of the ice sheets. For example, dark purple areas over Ellesmere Island and Baffin Island show the immediate inception of the ice sheets there, whereas the light orange colours in southern Scandinavia indicate that ice covered these regions from ~30 ka. In North America, the ice sheets incept from the North American Cordillera and Eastern Canada forming two large ice domes. In Eurasia, ice sheets incept at the
200 islands surrounding the Barents Sea. Little evidence exists on the inception phase of the LGC, since later glaciations tend to have removed most geological evidence. Modelling studies based on geological evidence, such as e.g., Bahadory et al. (2021) and Dalton et al. (2022), suggest that the North American ice sheet incepted at Ellesmere Island and the Canadian Cordillera, which agrees reasonably well for each simulation except for COSMOS forcing.

Between 120 and 60 ka, simulations forced with MPI and IPSL output have a comparatively large sea level
205 contribution (Fig. 3a). This can also be seen in the ice evolution (Fig. 4) for MPI and IPSL forcing leading to a large extent of the Baffin and Innuitian ice sheets during the inception phase of the ice sheets. Similarly, MPI forcing resulted in a large extent of the Barents-Kara ice sheets at the onset of the LGC. Since each simulation was forced by the same prescribed CO_2 and insolation, this is a result of the climate forcing and internal feedback processes.

Climate
of the Past
Discussions

Fig. 5 shows the LGM-PI temperature differences in the ice-sheet model domains. Shown here is that regions
210   with large ice extent at the early parts of the simulations correspond generally well to large LGM-PI temperature
differences. The LGM and PI temperatures are linearly interpolated with respect to prescribed CO_2 and albedo.
Therefore, the same change in CO_2 and albedo results in a larger temperature change with increasing LGM-PI
temperature difference provided by the GCMs.

Fig. 6 depicts ice thickness at LGM, showing that the ice extent varies considerably with climate forcing. In
215   North America, the differences in extent are mostly located along the southern margins. In the Eurasian ice sheet, the
differences are in Western Europe. Although in reality the British Isles were covered by glacial ice at LGM (e.g., Abe-
Ouchi et al., 2015, Batchelor et al., 2019), this only occurs in the simulation with MIROC forcing. Though this is
accompanied with a large ice volume compared to Simms et al., 2019 (see Fig. 3d). IPSL and COSMOS forcing lead to
limited LGM ice extent south of the Scandinavian mountains, which does not match paleo-reconstructions (e.g., Abe-
220   Ouchi et al., 2015, Batchelor et al., 2019). Fig. 7 shows LGM temperature and compares it to the extent of the ice sheet
simulations. This figure indicates that low LGM summer temperatures tend to match ice extent well, which is in line
with Niu et al. (2019). This is to be expected considering that temperature is a key player in the SMB by affecting the
amount of melt, refreezing and snowfall.

225   We are able to capture the LGM sea level (Simms et al., 2019) and extent (Abe-Ouchi et al., 2015) well using the climate
matrix method. While we tuned ice volume towards Simms et al. (2019), the extent of the LGM ice sheet is smaller
compared to Abe-Ouchi et al. (2015). The interior of the Laurentide ice sheet in our simulations has a thickness over
4000 meters, exceeding the thickness of the ICE6G-C reconstruction by Peltier et al. (2015). This suggests that not
enough ice is transported from the interior towards the margin, resulting in a small extent and large thickness in the
230   interior.

3.2 Ice sheet – climate feedbacks

Here we investigate the effect of the albedo-temperature and topography-precipitation feedbacks. We present two
simulations using the PMIP3-Ensemble forcing, which differ in their use of either the glacial index or the climate matrix
method.

235

Fig. 8c and 8d compare when the first ice accumulates in regions for the glacial index and climate matrix methods. In
the Eurasian ice sheet, which incepts mostly in the Barents-Kara Sea region, more domes are formed in the glacial index
method. This difference in the number of domes is even more pronounced in North America. Using the climate matrix
method, only the Laurentide and Cordilleran ice domes develop, which merge around 40 ka. In the glacial index method,

240   many smaller domes are formed in the Keewatin, Baffin and Cordilleran regions. The ice domes in the glacial index method simulations have much more irregular shapes compared to the smoother margins of the climate matrix ice domes. This North American ice sheet with few inception regions in the climate matrix method agrees better with studies conducted with geological constraints (e.g., Batchelor et al., 2019, Dalton et al., 2022).

        This difference in inception between the glacial index method and the climate matrix method is due to the
245   feedback processes. An ice sheet, which has a high albedo, creates a regionally cold climate enhancing ice growth. In regions without snow or ice, albedo is low leading to higher temperatures inhibiting ice inception. This feedback process is included in the climate matrix method, which separates temperature change caused by albedo and insolation, and CO_2. Consequently, the albedo in the ice-sheet model has a pronounced influence on temperature. In the glacial index method temperature is only affected by CO_2 and does not account for albedo changes. Hence, the glacial index method
250   underestimates (overestimates) cooling in high (low) albedo regions.

        Fig. 9 shows the sea level contribution of the Northern Hemisphere ice sheets over time. Ice volume at LGM is slightly higher in the glacial index method (110 m.s.l.e.) compared to the climate matrix method (96 m.s.l.e.). Accordingly, the glacial index method has larger volumes for the North American (Fig. 9b) and Eurasian (Fig. 9c) ice sheets. Ice thickness at LGM is shown in Fig. 8a,b. The Eurasian ice sheet in the glacial index method has more ice
255   covering the British Islands, but less in the Barents Sea region. The North American ice sheet margin extents more towards the south in the glacial index method. The smaller volume in the climate matrix method is mostly caused by the temperature-albedo interaction. In the climate matrix method, temperature and precipitation are only equal to the LGM time slice when CO_2, albedo and topography are the same as the ice sheet reconstruction. Since the ice sheet extent in the climate matrix method is smaller than LGM compared to the reconstruction, albedo is too low and consequentially
260   temperature is too high. Therefore, at LGM, the temperature in the ice-sheet model is higher compared to the LGM climate forcing. In the glacial index method, when CO_2 levels are equal to LGM the climate forcing is equal to LGM as well. Therefore, in these simulations, the LGM volume is higher in the glacial index method.

        After the LGM, the Eurasian and North American ice sheets retreat. Fig. 10b shows the modelled sea level contribution rate during the LGC. While sea level contribution rates reach negative values at approximately the same
265   time, the climate matrix method finishes retreating later (5 ka) compared to the glacial index method (8 ka). Furthermore, Fig. 10a compares sea level contribution to CO_2, with timestamps indicated in the figure. Considering an arbitrary threshold of 5 mm/yr shows that the glacial index method retreat rate accelerates faster at lower CO_2 concentrations (18 ka, 225 ppm) compared to the climate matrix method (16 ka, 240 ppm). This indicates a lower CO_2 threshold for retreat in the glacial index method. The peak sea level rate in the glacial index method is higher and earlier in the glacial index
270   method, with a decrease of 32 mm/yr (11 ka) compared to 19 mm/yr (8 ka) in the climate matrix method. This is because when the CO_2 increases rapidly, low temperatures persist longer in the climate matrix method due to the high albedo of

the large ice sheet, while the response of the glacial index method is instantaneous. The climate matrix has the tendency to maintain the ice sheet as it is, and does not warm as quickly, resulting in lower retreat rates.

4. Discussion and Conclusion

275   In this study we simulated the Northern Hemisphere ice sheets of the LGC using an ice-sheet model. Our aim was to investigate the sensitivity to paleoclimate forcing, and to assess the effects of the ice sheet – climate interaction.

We used climate forcing obtained from of the PMIP3 ensemble to investigate the sensitivity of a climate matrix and glacial index method. We find that the differences in ice volume due to climate forcing exceeds the differences caused by the transient climate interpolation method. Several PMIP3 models yield unrealistic ice sheet configurations.

280   Despite choosing only a subset of the PMIP3 simulations, sea level contribution of the Northern-Hemisphere ice sheets still shows a considerable range, between 74 – 113 meters. These large differences are in line with findings by Niu et al. (2019) and Alder & Hostetler (2019), and is not exclusively found with PMIP3 forcing, but also for the first PMIP ensemble by Charbit et al. (2007). Our study additionally used the climate matrix method instead of only the glacial index method used by Charbit and Niu, showing that even when including atmospheric feedback processes, the range in

285   sea level contribution is still large. As originally suggested by Niu et al. (2019), cold LGM summer temperatures generally correspond well with areas of LGM ice cover when using PMIP3 climate forcing to simulate the LGC. This is caused by the fact that high ablation rates at the margin inhibit ice advance and ablation rates depends strongly on temperature.

In this study, we compared the glacial index and climate matrix method with a realistic experiment for the first

290   time. The LGC simulations using the glacial index and climate matrix method were conducted with the same climate forcing, PMIP3-Ensemble. The glacial index method and climate matrix methods yield similar LGM ice volumes, but show a much larger difference in ice evolution. Generally, the climate matrix method incepts at fewer domes, with the few domes that form being larger and more regularly shaped compared to the glacial index method. In the glacial index method, many more smaller domes form, often far away from the main ice sheet centres. In both methods, the domes

295   gradually merge to form one big Eurasian or Laurentide ice sheet. The difference in inception is due to the albedo-temperature feedback, where temperatures in the climate matrix method are low along ice margins and high in regions with low albedo. In the climate matrix method this enhances ice growth close to ice margins and inhibits ice inception of new domes in regions with low albedo. We find that the ice sheets, especially the Laurentide ice sheet, deglaciate faster in the glacial index method compared to the climate matrix method. This is attributed to the albedo-temperature

300   feedback, as the high albedo of the ice sheet can maintain colder temperatures at the onset of deglaciation.

However, neither the glacial index nor climate matrix method match global eustatic sea level evolution well during the LGM when comparing it to reconstructions (e.g., Gowan et al., 2021). In both the glacial index and climate

matrix methods ice volume generally increases gradually, while studies that depend more on geological constrains such as Batchelor et al., 2019 and Dalton et al., 2022 suggest a more dynamic change in ice volume and area for the North

305 American ice sheet. Our method is unable to capture the sea level rise during MIS-3, when most of the Eurasian ice sheet is lost. This indicates that we are missing forcing and or feedback processes that result in melt before the final deglaciation at 18 ka. This may include a stronger effect of insolation on mass balance. This is perhaps related to the annually averaging ignoring seasonal fluctuations. Since we use only LGM and PI time slices, and only interpolate not simulate the climate, we do not capture threshold behaviour such as the closure of the Canadian Artic Archipelago

310 gateways (Löfverström et al., 2022) or processes not captured in LGM and PI time slices such as Dansgaard/Oeschger and Heinrich events and their impact on climate (Claussen et al., 2003). To capture this, transient GCM simulation are required rather than any temporal interpolation method as used here.

Appendix A: Surface mass balance model

We use IMAU-ITM to calculate surface mass balance (Berends et al., 2018). This SMB scheme requires temperature

315 and precipitation fields that we obtain from the GCM fields after applying the methods described in appendix C and D. Monthly melt in IMAU-ITM is parameterised using Bintanja et al. (2002) and calculated as following:

$$Melt(x,y,m) = (c_1 (T(x,y,m) - T0) + c_2 (1 - \alpha(x,y,m)) Q_{TOA}(x,y,m) - c_3)(s/yr) / (L_{fusion} 12000), \quad (1)$$

Here, the melting temperature of ice ($T0$) is 273.16 K, Q_{TOA} is the insolation at the top of the atmosphere from Laskar et al. (2004) in W/m^2 and L_{fusion} is the latent heat of fusion in J/kg. Values for c_1, c_2 and c_3 are tuning parameters

320 shown in Table A1. Albedo (α) is calculated internally as follwing:

$$\alpha_{surface}(x,y,m) = \alpha_{snow} - (\alpha_{snow} - \alpha_{background}) e^{-15 FirnDepth(m-1,x,y) - 0.015 MeltPreviousYr(x,y)}, \quad (2)$$

Here, $\alpha_{background}$ is 0.1 for water, 0.2 for land, 0.5 for bare ice, and α_{snow} is 0.85 and MeltPreviousYr is the melt of the previous model year. Firn depth is calculated using the amount of snowfall that has been added without melting and is capped at 10 meters. For snowfall we use a temperature-based snow rain partitioning from Ohmura et al. (1999).

325
$$snowfraction = 0.725 * \left(1 - \frac{atan\frac{(T(x,y,m)-T0)}{5.95}}{1.8566}\right), \quad (3)$$

The $snowfraction$ is the fraction of precipitation (P) that falls as snow with the remainder falling as rain. To calculate the total accumulation, we need refreezing. This is calculated using the approach by Huybrechts & de Wolde, 1999:

$$SuperImposedWater(x,y,m) = \max\{0, 0.012(T0 - T(x,y,m))\}, \quad (4)$$

$$LiquidWater(x,y,m) = RainFall(x,y,m) + Melt(x,y,m), \quad (5)$$

330
$$Refreezing(x,y,m) = \min\{\min\{SuperImposedWater(x,y,m), LiquidWater(x,y,m)\}, P(x,y,m)\}, \quad (6)$$

Using the previous calculated snowfall, rainfall, refreezing and melt, the SMB can be obtained:

$$SMB(x, y, m) = Snowfall(x, y, m) + Refreezing(x, y, m) - Melt(x, y, m). \quad (7)$$

Table A1. The parameters used to calculate ablation in the approach by Bintanja et al. (2002). The surface mass balance parameters were tuned towards the PMIP3-Ensemble simulation to obtain ice sheets that agree well with Simms et al., 2019.

Domain	c1 $(m\ yr^{-1}\ K^{-1})$	c2 $(m^3 J^{-1})$	c3 $(m^3 J^{-1}$; Preliminary Experiments)	c3 $(m^3 J^{-1}$; Tuned)
North America	10	0.513	18	18
Eurasia	10	0.513	34.5	20
Greenland	10	0.513	24	24

Appendix B: Climate forcing selection and SMB tuning

Niu et al. (2019) and Alder & Hostetler (2019) have shown that there are large differences in the modelled ice sheets between the different PMIP3 climates. For our ice sheet simulations, we would ideally use climate forcing with which we can obtain a good representation of the ice sheets at LGM. First, we conducted simulations forced with all nine available PMIP3 simulations using an untuned ablation (see Table A1), these are shown in Figure B1. Since we obtained large differences between the simulations forced by the individual PMIP3 ensemble members, some deviating substantially from reconstructions, we used a smaller selection of models.

To make a selection of the PMIP3 climates, we compared the simulated ice sheet extent to the reconstruction from Abe-Ouchi et al. (2015). This reconstruction was used as a prescribed LGM ice extent in the climate model simulations. We compare the ice sheet model and reconstruction at LGM to compute the percentage of too large and too small ice extent. For example, the simulation with MRI forcing resulted in a small Eurasian ice sheet. Ice in the simulation does not cover 91% of the reconstructed extent. Some ice is also found outside the extent of the reconstruction. Therefore, MRI climate forcing also resulted in 1% too much ice extent outside the reconstruction. These percentages of too little and too much ice is listed in Table B1. We added these values together and applied a threshold of 40% to select the climate forcing. MIROC, IPSL, COSMOS and MPI stayed below this threshold for both the Eurasian and North American ice sheets. The other models are above this threshold and are excluded from further study. A climate forcing was made from the mean of this selection and called PMIP3-Ensemble (4 GCMs). Using this ensemble climate, the SMB model was tuned towards sea level by Simms et al. (2019).

Table B1. Shown here are the percentage of ice extent missing added to the percentages of ice extent that exceeds Abe-Ouchi et al. (2015) reconstruction. Lower percentages indicate a better match to Abe-Ouchi et al. (2015). Simulations that stayed below the 40% threshold are depicted in bold.

Climate Model	Eurasia Too little	Eurasia Too much	Eurasia Total	North America Too little	North America Too much	North America Total
CCSM4	0.32	0.21	0.53	0.89	0.00	0.89
CNRM-CM5	0.97	0.00	0.97	0.99	0.00	0.98
COSMOS-ASO	0.18	0.15	**0.33**	0.33	0.00	**0.33**
FGOALS-g2	0.11	0.37	0.48	0.44	0.01	0.45
GISS-E2-R	0.13	1.37	1.50	0.77	0.03	0.79
IPSL-CM5A-LR	0.24	0.04	**0.28**	0.26	0.00	**0.26**
MIROC-ESM	0.06	0.28	**0.34**	0.17	0.02	**0.19**
MPI-ESM-P	0.10	0.16	**0.26**	0.25	0.00	**0.25**
MRI-CGCM3	0.91	0.01	0.92	0.97	0.00	0.97
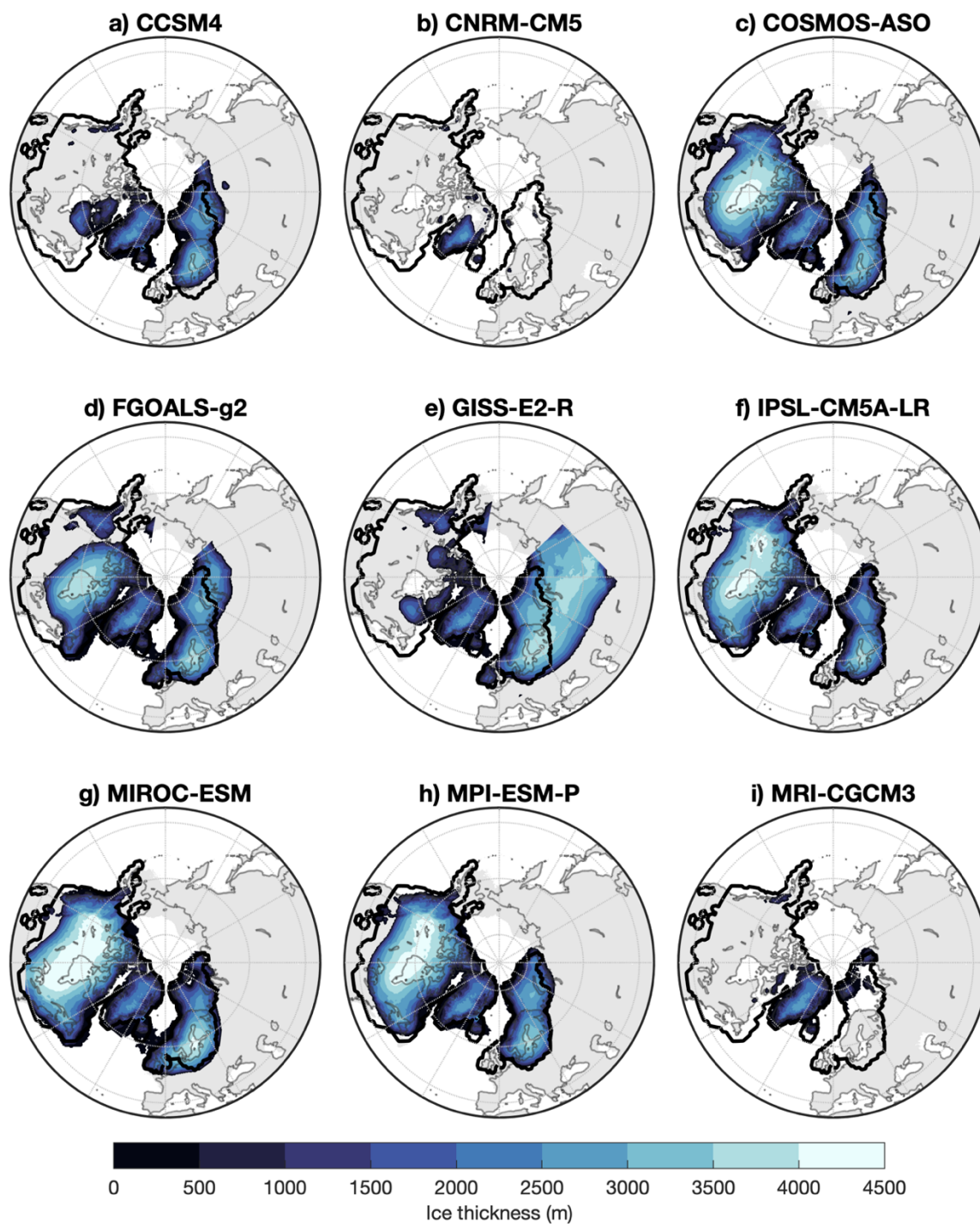
Figure B1. LGM ice thickness of nine LGC simulations. The ice sheet model was forced by the nine available PMIP3 climates interpolated using the climate matrix method.

Appendix C: Bias correction

We apply a correction to the climate forcing to correct for biases in the climate models. First, we calculate the difference between the PI climate from the General Circulation Models (GCM) and observed climate from ERA40 (Uppala et al., 2005). These differences are then applied to the LGM and PI climate forcing.

365   To apply the bias correction for temperature, we first need to account for differences in topography between the model and observation data. Here we apply a lapse rate (λ) correction to calculate temperature at sea level.

$$T_{obs,SL}(x,y,m) = T_{obs,PD}(x,y,m) + Hs_{obs,PD}(x,y)\,\lambda(x,y), \tag{8}$$

$$T_{GCM,SL}(x,y,m) = T_{GCM,PD}(x,y,m) + Hs_{GCM,PD}(x,y)\,\lambda(x,y), \tag{9}$$

Using the temperature at sea level from observations ($T_{obs,SL}$) and the climate model ($T_{GCM,SL}$), we can calculate the

370 difference between observed and modelled temperature.

$$T_{GCM,bias}(x,y,m) = T_{GCM,SL}(x,y,m) - T_{obs,SL}(x,y,m), \tag{10}$$

$T_{GCM,bias}$ represents the bias between modelled and observed data. We can apply this to the LGM and PI time slices to obtain a bias-corrected temperature.

$$T_{GCM,corr}(x,y,m) = T_{GCM}(x,y,m) - T_{GCM,bias}(x,y,m), \tag{11}$$

375 Here, T_{GCM} is the GCM output, either PI or LGM, while $T_{GCM,corr}$ the bias corrected GCM data.

       For precipitation (P), we use the ratio between model and observed data instead. First, we calculate the bias between model and observational data directly.

$$P_{GCM,bias}(x,y,m) = P_{GCM,PI}(x,y,m) \,/\, P_{obs,PI}(x,y,m), \tag{12}$$

Secondly, we apply this bias correction on the GCM data.

380 $$P_{GCM,corr}(x,y,m) = P_{GCM}(x,y,m) \,/\, P_{GCM,bias}(x,y,m), \tag{13}$$

After applying these corrections, we have obtained bias corrected temperature and precipitation fields for LGM and PI.

Appendix D: Climate interpolation

The glacial index and climate matrix methods are used to interpolate between the climate model LGM and PI time slices. As a result, both interpolation methods produce a transiently changing climate throughout the LGC. Here we apply the

385 method by Berends et al. (2018), for which we use the bias corrected fields for temperature and precipitation. To compute the interpolated temperature and precipitation forcing in both the glacial index and climate matrix method, we use the following two equations:

$$T_{ref}(x,y,m) = w_{tot}(x,y)\,T_{PI,corr}(x,y,m) + \big(1 - w_{tot}(x,y)\big)\,T_{LGM,corr}(x,y,m), \tag{14}$$

$$P_{ref} = e\left(w_{PI}(x,y)\log\big(P_{PI,corr}(x,y,m)\big) + w_{LGM}(x,y)\log\big(P_{LGM,corr}(x,y,m)\big)\right), \tag{15}$$

390 Here T_{ref} and P_{ref} are the temperature and precipitation climate forcing respectively. The weights for the interpolation are represented by w_{tot}, w_{LGM} and w_{PI}. The calculation for these interpolation weights determines the difference between the climate matrix and glacial index method.

In the glacial index method w_{tot}, w_{LGM} and w_{PI} are calculated with only prescribed CO_2.

$$w_{CO2} = (CO_2 - CO_{2_{LGM}}) / (CO_{2_{PI}} - CO_{2_{LGM}}),$$ (16)

395 Here, CO_2 represents the prescribed CO_2 concentration obtained from Bereiter et al. (2015) at the current model time-step. LGM and PI CO_2 concentrations are 190 and 280 ppm respectively. Note here that w_{CO2} is a scalar. In the glacial index method, w_{CO2} is equal to w_{tot}, w_{PI}, and , $(1 - w_{LGM})$. Since CO_2 is the same across the entire globe, not only are these values uniform, but they are also the same for each domain. There is no interaction between the ice sheet model and the interpolation.

400 The climate matrix method expands on the glacial index method by including a parameterised temperature-albedo and precipitation-topography feedback. For temperature, w_{tot} is calculated using both prescribed CO_2 and absorbed insolation. The annual absorbed insolation is calculated as following:

$$I_{abs}(x,y) = \sum_{m=1}^{12} Q_{TOA}(x,y,m) \left(1 - \alpha_{surface}(x,y,m)\right),$$ (17)

Here Q_{TOA} is the insolation at the top of the atmosphere, for which we use prescribed forcing from Laskar et al. (2004).

405 Albedo (α) is calculated internally, more details on this is described in appendix A. To calculate annual I_{abs}, we use the sum of the monthly I_{abs}. We can use this to calculate the interpolation weights for the absorbed insolation.

$$w_{ins}(x,y) = (I_{abs}(x,y) - I_{abs,LGM}(x,y)) / (I_{abs,PI}(x,y) - I_{abs,LGM}(x,y)),$$ (18)

$I_{abs_{PI}}$ and $I_{abs_{LGM}}$ are the reference PI and LGM absorbed insolation respectively. This reference albedo is calculated using equation 2, where we use PI and LGM for Q_{TOA} and $\alpha_{surface}$. To calculate albedo at LGM, we apply the

410 topography, ice mask, and land mask from Abe-Ouchi et al. (2015) and run the SMB model to obtain the albedo change due to snow. Since albedo and insolation vary across the domain, w_{ins} is not uniform. To obtain the regional effect of albedo on temperature, we calculate the mean w_{ins} ($w_{ins,av}$) and w_{ins} with a gaussian smoothening of 200 km ($w_{ins,smooth}$). Using these insolation weights, we can calculate the interpolation weight (w_{ice}) resulting from ice interactions.

415 In the North America and Eurasia domain:

$$w_{ice}(x,y) = \frac{w_{ins}(x,y) + 3\,w_{ins,smooth}(x,y) + 3\,w_{ins,av}(x,y)}{7},$$ (19)

$$w_{tot,T}(x,y) = \frac{(w_{CO2}(x,y) + w_{ice}(x,y))}{2},$$ (20)

In the Greenland domain:

$$w_{ice}(x,y) = \frac{w_{ins,smooth}(x,y) + 6\,w_{ins,av}}{7},$$ (21)

Climate
of the Past

Open Access

Discussions

EGU

420
$$w_{tot,T}(x,y) = (3\,w_{CO2}(x,y) + w_{ice}(x,y))/4, \tag{22}$$

The field w_{tot} is used in equation 14 to calculate temperature.

Precipitation in the climate matrix method is only dependent on surface topography. First, we calculate the total change in surface topography (Hs) between LGM and PI.

425
$$w_{tot,P}(x,y) = \left(\sum Hs\,(x,y) - \sum Hs_{PI}(x,y)\right) / \left(\sum Hs_{LGM}(x,y) - \sum Hs_{PI}(x,y)\right), \tag{23}$$

For regions within the ice extent of Abe-Ouchi et al. (2015), we calculate the regional change in topography.

$$w_{LGM,Hs}(x,y) = \frac{Hs_{ISM}(x,y) - Hs_{GCM\,PI}(x,y)}{Hs_{GCM,LGM}(x,y) - Hs_{GCM,PI}(x,y)}\,w_{tot,P}(x,y), \tag{24}$$

In regions that are outside the bounds of this ice extent $w_{LGM,Hs}$ is equal to $w_{tot,P}$. We multiply w_{LGM} with w_{tot} to account for the regional effect on precipitation due to a change in surface topography.

430
$$w_{LGM}(x,y) = w_{LGM,Hs}(x,y)\,w_{tot,P}(x,y), \tag{25}$$

This w_{LGM} is used in equation 15 to calculate precipitation. Note here that precipitation is not uniform. Only as the ice sheet increases in thickness, Hs increases which raises w_{LGM}.

Code availability: The source code of IMAU-ICE is maintained on GitHub at https://github.com/IMAU-paleo/IMAU-
435 ICE/tree/Last_Glacial_Cycle_PMIP3. The exact version used in this study (including makefiles, compiling scripts, run scripts, config files for all the simulations presented here, and MATLAB scripts for creating the figures) will be made available at Zenodo (https://zenodo.org) at a later point. Please note that model simulations cannot be conducted without input files for CO_2, climate and initial topography. For more information, contact the corresponding author.

Data availability: The simulation output shown in this study will be made available at a later point at Zenodo
440 (https://zenodo.org) for a 10 kyr output frequency. Output every 1 kyr as well as additional fields can be requested by contacting the corresponding author.

Author contributions. MS has conducted the simulations and written the manuscript. Experimental set-up was created
445 by RW, CB and MS. Model support has been provided by CB and LS. All authors have helped analysing the results and contributed to the text.

Competing interest. The authors declare that they have no conflict of interest

Climate
of the Past
Discussions

Open Access

EGU

References

Abe-Ouchi, A., Segawa, T., and Saito, F.: Climatic Conditions for modelling the Northern Hemisphere ice sheets throughout
460   the ice age cycle, Clim. Past, 3, 423–438, https://doi.org/10.5194/cp-3-423-2007, 2007.

Abe-Ouchi, A., Saito, F., Kageyama, M., Braconnot, P., Harrison, S. P., Lambeck, K., Otto-Bliesner, B. L., Peltier, W. R., Tarasov, L., Peterschmitt, J.-Y., and Takahashi, K.: Ice-sheet configuration in the CMIP5/PMIP3 Last Glacial Maximum experiments, Geosci. Model Dev., 8, 3621–3637, https://doi.org/10.5194/gmd-8-3621- 2015, 2015.

Alder, J. R. and Hostetler, S. W.: Applying the Community Ice Sheet Model to evaluate PMIP3 LGM climatologies over the
465   North American ice sheets, Clim. Dynam., 53, 2807–2824, https://doi.org/10.1007/s00382-019-04663-x, 2019.

Annan, J. D. and Hargreaves, J. C.: A new global reconstruction of temperature changes at the Last Glacial Maximum, Clim. Past, 9, 367–376, https://doi.org/10.5194/cp-9-367-2013, 2013.

Argus, D. F. and Peltier, W. R.: Constraining models of postglacial rebound using space geodesy: a detailed assessment of model ICE-5G (VM2) and its relatives, Geophys. J. Int., 181, 697–723, https://doi.org/10.1111/j.1365-246X.2010.04562.x,
470   2010.

Bahadory, T., Tarasov, L., and Andres, H.: Last glacial inception trajectories for the Northern Hemisphere from coupled ice and climate modelling, Clim. Past, 17, 397–418, https://doi.org/10.5194/cp-17-397-2021, 2021.

Batchelor, C. L., Margold, M., Krapp, M., Murton, D. K., Dalton, A. S., Gibbard, P. L., Stokes, C. R., Murton, J. B., and Manica, A.: The configuration of Northern Hemisphere ice sheets through the Quaternary, Nat. Commun., 10, 1–10, 2019.

475 Bereiter, B., Eggleston, S., Schmitt, J., Nehrbass-Ahles, C., Stocker, T. F., Fischer, H., Kipfstuhl, S., and Chappellaz, J.: Revision of the EPICA Dome C CO2 record from 800 to 600 kyr before present, Geophys. Res. Lett., 42, 542–549, https://doi.org/10.1002/2014GL061957, 2015.

Berends, C. J., de Boer, B., and van de Wal, R. S. W.: Application of HadCM3@Bristolv1.0 simulations of paleoclimate as forcing for an ice-sheet model, ANICE2.1: set-up and benchmark experiments, Geosci. Model Dev., 11, 4657–4675,
480   https://doi.org/10.5194/gmd-11-4657-2018, 2018.

Berends, C. J., Goelzer, H., Reerink, T. J., Stap, L. B., and van de Wal, R. S. W.: Benchmarking the vertically integrated ice-sheet model IMAU-ICE (version 2.0), Geosci. Model Dev., 15, 5667–5688, https://doi.org/10.5194/gmd-2021-352, 2022.

Bintanja, R., van de Wal, R. S. W., and Oerlemans, J.: Global ice volume variations through the last glacial cycle simulated by a 3-D ice dynamical model, Quater. Int., 95–96, 11–23, 2002.

485 Braconnot, P., Harrison, S. P., Otto-Bliesner, B. L., Abe-Ouchi, A., Jungclaus, J. H., and Peterschmitt, J.-Y.: The Paleoclimate Modeling Intercomparison Project contribution to CMIP5, CLIVAR Exchanges, 56, 15–19, 2011.

Brady, E. C., Otto-Bliesner, B. L., Kay, J. E., and Rosenbloom, N.: Sensitivity to Glacial Forcing in the CCSM4, J. Climate, 26, 1901–1925, https://doi.org/10.1175/JCLI-D-11-00416.1, 2013.

Budich, R., Gioretta, M., Jungclaus, J., Redler, R., and Reick, C.: The MPI-M Millennium Earth System Model: An assembling 490 guide for the COSMOS configuration, Tech. rep., Max-Planck Institute for Meteorology, Hamburg, Germany, 2010.

Bueler, E. and van Pelt, W.: Mass-conserving subglacial hydrology in the Parallel Ice Sheet Model version 0.6, Geosci. Model Dev., 8, 1613–1635, https://doi.org/10.5194/gmd-8-1613-2015, 2015.

Charbit, S., Ritz, C., Philippon, G., Peyaud, V., and Kageyama, M.: Numerical reconstructions of the Northern Hemisphere ice sheets through the last glacial-interglacial cycle, Clim. Past, 3, 15–37, https://doi.org/10.5194/cp-3-15-2007, 2007.

495 Clark, P. U., Alley, R. B., and Pollard, D.: Northern Hemisphere Ice-Sheet Influences on Global Climate Change, Science, 286, 1104–1111, https://doi.org/10.1126/science.286.5442.1104, 1999.

Claussen, M., Ganopolski, A., Brovkin, V., Gerstengarbe, F.-W., and, Werner, P.: Simulated global-scale response of the climate system to Dansgaard/Oeschger and Heinrich events, Clim. Dynam., 21, 361–370, 2003.

Dalton, A. S., Stokes, C. R., and Batchelor, C. L.: Evolution of the Laurentide and Innuitian ice sheets prior to the Last Glacial 500 Maximum (115 ka to 25 ka), Earth Sci. Rev., 224, 103875, https://doi.org/10.1016/j.earscirev.2021.103875, 2022.

de Boer, B., van de Wal, R., Lourens, L. J., Bintanja, R., and Reerink, T. J.: A continuous simulation of global ice volume over the past 1 million years with 3-D ice-sheet models, Clim. Dynam., 41, 1365–1384, 2013.

de Boer, B., Stocchi, P., and van de Wal, R. S. W.: A fully coupled 3-D ice-sheet–sea-level model: algorithm and applications, Geosci. Model Dev., 7, 2141–2156, https://doi.org/10.5194/gmd-7-2141- 2014, 2014.

505 Dufresne, J.-L., Foujols, M.-A., Denvil, S., Caubel, A., Marti, O., Aumont, O., Balkanski, Y., Bekki, S., Bellenger, H., Benshila, R., Bony, S., Bopp, L., Braconnot, P., Brockmann, P., Cadule, P., Cheruy, F., Codron, F. F., Cozic, A., Cugnet, D., de Noblet, N., Duvel, J.-P., Ethé, C., Fairhead, L., Fichefet, T., Flavoni, S., Friedlingstein, P., Grandpeix, J.-Y., Guez, L., Guilyardi, E., Hauglustaine, D., Hourdin, F., Idelkadi, A., Ghattas, J., Joussaume, S., Kageyama, M., Krinner, G., Labetoulle, S., Lahellec, A., Lefèbvre, M.-P., Lefèvre, F., Lévy, C., Li, Z. X., Lloyd, J., Lott, F., Madec, G., Mancip, M., 510 Marchand, M., Masson, S., Meurdesoif, Y., Mignot, J., Musat, I., Parouty, S., Polcher, J., Rio, C., Schulz, M., Swingedouw, D., Szopa, S., Talandier, C., Terray, P., and Viovy, N.: Climate change projections using the IPSL-CM5 Earth System Model: from CMIP3 to CMIP5, Clim. Dynam., 40, 2123–2165, https://doi.org/10.1007/s00382-012-1636-1, 2013.

Feldmann, J., Albrecht, T., Khroulev, C., Pattyn, F., and Levermann, A.: Resolution-dependent performance of grounding line motion in a shallow model compared to a full-Stokes model according to the MISMIP3d intercomparison, J. Glaciol., 60,

515   353–360, 2014.

Fettweis, X., Hofer, S., Krebs-Kanzow, U., Amory, C., Aoki, T., Berends, C. J., Born, A., Box, J. E., Delhasse, A., Fujita, K., Gierz, P., Goelzer, H., Hanna, E., Hashimoto, A., Huybrechts, P., Kapsch, M.-L., King, M. D., Kittel, C., Lang, C., Langen, P. L., Lenaerts, J. T. M., Liston, G. E., Lohmann, G., Mernild, S. H., Mikolajewicz, U., Modali, K., Mottram, R. H., Niwano, M., Noël, B. P. Y., Ryan, J. C., Smith, A., Streffing, J., Tedesco, M., van de Berg, W. J., van den Broeke, M. R., van de Wal,

520   R. S. W., van Kampenhout, L., Wilton, D., Wouters, B., Ziemen, F., and Zolles, T.: GrSMBMIP: intercomparison of the modelled 1980-2012 surface mass balance over the Greenland Ice Sheet, The Cryosphere 14, 3935-3958, https://doi.org/10.5194/tc-14-3935-2020, 2020.

Fox-Kemper, B., Hewitt, H. T., Xiao, C., Adalgeirsdottir, G., Drijfhout, S. S., Edwards, T. L., Golledge, N. R., Hemer, M., Kopp, R. E., Krinner, G., Mix, A., Notz, D., Nowicki, S., Nurhati, I. S., Ruiz, L., Sallée, J.-B., Slangen, A. B. A., and Yu,

525   Y.: Ocean, Cryosphere and Sea Level Change, in: Climate Change 2021: The Physical Science Basis. Contribution of Working Group 1 to the Sixth Assessment Report of the Intergovernmental Panel on Climate change, edited by: Masson-Delmotte, V., Zhai, P., Pirani, A., Connors, S. L., Péan, C., Berger, S., Caud, N., Chen, Y., Goldfarb, L., Gomis, M. I., Huang, M., Leitzell, K., Lonnoy, E., Matthes, J. B. R., Maycock, T. K., Waterfield, T., Yelekci, O., Yu, R., and Zhou, B., Cambridge University Press, Cambridge, United Kingdom and New York, NY, USA, 1211–1362,

530   https://doi.org/10.1017/9781009157896.011, 2021.

Ganopolski, A., Calov, R., and Claussen, M.: Simulation of the last glacial cycle with a coupled climate ice-sheet model of intermediate complexity, Clim. Past, 6, 229–244, https://doi.org/10.5194/cp-6-229-2010, 2010.

Goldberg, D. N.: A variationally derived, depth-integrated approximation to a higher-order glaciological flow model, J. Glaciol., 57, 157–170, 2011.

535   Gowan, E. J., Zhang, X., Khosravi, S., Rovere, A., Stocchi, P., Hughes, A. L. C., Gyllencreutz, R., Mangerud, J., Svendsen, J.-I., and Lohmann, G.: A new global ice sheet reconstruction for the past 80000 years, Nat. Commun., 12, 1199, https://doi.org/10.1038/s41467-021-21469-w, 2021.

Huybrechts, P. and de Wolde, J.: The dynamic response of the Greenland and Antarctic ice sheets to multiple-century climatic warming, J. Climate, 1, 2169–2188, 1999.

540   Janssens, I. and Huybrechts, P.: The treatment of meltwater retention in mass-balance parameterizations of the Greenland ice sheet, in: Ann. Glaciol., 31, 2000, edited by: Steffen, K., Ann. Glaciol., Int Glaciological Soc, Cambridge, 133–140, 2000.

Jungclaus, J., Giorgetta, M., Reick, C., Legutke, S., Brovkin, V., Crueger, T., Esch, M., Fieg, K., Fischer, N., Glushak, K., Gayler, V., Haak, H., Hollweg, H.-D., Kinne, S., Kornblueh, L., Matei, D., Mauritsen, T., Mikolajewicz, U., Müller, W., Notz, D., Pohlmann, T., Raddatz, T., Rast, S., Roeckner, E., Salzmann, M., Schmidt, H., Schnur, R., Segschneider, J., Six,

545   K., Stockhause, M., Wegner, J., Widmann, H., Wieners, K.-H., Claussen, M., Marotzke, J., and Stevens, B.: CMIP5

simulations of the Max Planck Institute for Meteorology (MPI-M) based on the MPI- ESM-P model: The lgm experiment, served by ESGF, WDCC at DKRZ, https://doi.org/10.1594/WDCC/CMIP5.MXEPlg, 2012.

Lambeck, K., Purcell, A., Zhao, J., and Svensson, N.-O.: The Scandinavian Ice Sheet: from MIS 4 to the end of the Last Glacial Maximum, Boreas, 39, 410–435, https://doi.org/10.1111/j.1502- 3885.2010.00140.x, 2010.

550   Laskar, J., Robutel, P., Gastineau, M., Correia, A. C. M., and Levrard, B.: A long-term numerical solution for the insolation quantities of the Earth, Astron. Astrophys., 428, 261–285, 2004.

Leguy, G. R., Lipscomb, W. H., and Asay-Davis, X. S.: Marine ice sheet experiments with the Community Ice Sheet Model, The Cryosphere 15, 3229-3253, 2021.

Le Meur, E. and Huybrechts, P.: A comparison of different ways of dealing with isostasy: examples from modelling the
555   Antarctic ice sheet during the last glacial cycle, Ann. Glaciol., 23, 309–317, 1996.

Löfverström, M., Caballero, R., Nilsson, J., and Kleman, J.: Evolution of the large-scale atmospheric circulation in response to changing ice sheets over the last glacial cycle, Clim. Past, 10, 1453–1471, https://doi.org/10.5194/cp-10-1453-2014, 2014.

Löfverström, M., Thompson, D. M., Otto-Bliesner, B. L., and Brady, E. C.: The importance of Canadian Arctic Archipelago gateways for glacial expansion in Scandinavia, Nat. Geosci, 15, 482-488, https://doi.org/10.1038/s41561-022-00956-9,
560   2022.

Martin, M. A., Winkelmann, R., Haseloff, M., Albrecht, T., Bueler, E., Khroulev, C., and Levermann, A.: The Potsdam Parallel Ice Sheet Model (PISM-PIK) – Part 2: Dynamic equilibrium simulation of the Antarctic ice sheet, The Cryosphere, 5, 727–740, https://doi.org/10.5194/tc-5-727-2011, 2011.

Niu, L., Lohmann, G., Hinck, S., Gowan, E. J., and Krebs-Kanzow, U.: The sensitivity of Northern Hemisphere ice sheets to
565   atmospheric forcing during the last glacial cycle using PMIP3 models, J. Glaciol., 65, 645–661, https://doi.org/10.1017/jog.2019.42, 2019.

Ohmura, A., Calanca, P., Wild, M. and Anklin M.: Precipitation, accumulation and mass balance of the Greenland Ice sheet, Z. Gletscherkd. Glazialgeol., 35(1), 1–20, 1999.

Pausata, F. S. R., Li, C., Wettstein, J. J., Kageyama, M., and Nisancioglu, K. H.: The key role of topography in altering North
570   Atlantic atmospheric circulation during the last glacial period, Clim. Past, 7, 1089–1101, https://doi.org/10.5194/cp-7-1089-2011, 2011.

Peltier, W. R., Argus, D. F., and Drummond, R.: Space geodesy constrains ice age terminal deglaciation: The global ICE-6G_C(VM5a) model, J. Geophys. Res.-Sol. Ea., 120, 450–487, https://doi.org/10.1002/2014JB011176, 2015.

Pollard, D.: A retrospective look at coupled ice sheet-climate modelling, Climatic Change, 100, 173–194, 2010.

575   Roe, G. H. and Lindzen, R. S.: The Mutual Interaction between Continental-Scale Ice Sheets and Atmospheric Stationary Waves., J. Climate, 14, 1450–1465, 2001.

Simms, A. R., Lisiecki, L., Gebbie, G., Whitehouse, P. L., and Clark, J. F.: Balancing the last glacial maximum (LGM) sea-level budget, Quatern. Sci. Rev., 205, 143–153, https://doi.org/10.1016/j.quascirev.2018.12.018, 2019.
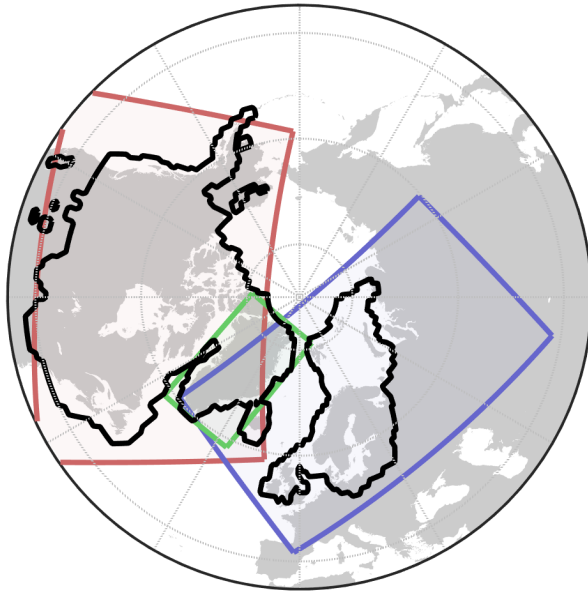
Smith, R. S. and Gregory, J.: The last glacial cycle: transient simulations with an AOGCM, Clim. Dynam., 38, 1545–1559,
580   https://doi.org/10.1007/s00382-011-1283-y, 2012.

Stap, L. B., van de Wal, R. S. W., de Boer, B., Bintanja, R., and Lourens, L. J.: Interaction of ice sheets and climate during the
       past 800000 years, Clim. Past, 10, 2135–2152, https://doi.org/10.5194/cp-10-2135-2014, 2014.

Stap, L. B., Berends, C. J., Scherrenberg, M. D., Van De Wal, R. S., and Gasson, E. G. (2022): Net effect of ice-sheet–
       atmosphere interactions reduces simulated transient Miocene Antarctic ice-sheet variability, The Cryosphere, 16, 1315–1332,
585   https://doi.org/10.5194/tc-16-1315-2022, 2022.

Sueyoshi, T., Ohgaito, R., Yamamoto, A., Chikamoto, M. O., Hajima, T., Okajima, H., Yoshimori, M., Abe, M., O'ishi, R.,
       Saito, F., Watanabe, S., Kawamiya, M., and Abe-Ouchi, A.: Set-up of the PMIP3 paleoclimate experiments conducted using
       an Earth system model, MIROC-ESM, Geosci. Model Dev., 6, 819–836, https://doi.org/10.5194/gmd-6-819-2013, 2013.

Tarasov, L., Dyke, A. S., Neal, R. M., and Peltier, W. R.: A data-calibrated distribution of deglacial chronologies for the North
590   American   ice   complex   from   glaciological   modeling,   Earth   Planet.   Sci.   Lett.,   315,   30–40,
       https://doi.org/10.1016/j.epsl.2011.09.010, 2012.

Ullman, D. J., LeGrande, A. N., Carlson, A. E., Anslow, F. S., and Licciardi, J. M.: Assessing the impact of Laurentide Ice
       Sheet topography on glacial climate, Clim. Past, 10, 487–507, https://doi.org/10.5194/cp-10-487-2014, 2014.

Uppala, S. M., Kållberg, P. W., Simmons, A. J., Andrae, U., da Costa Bechtold, V., Fiorino, M., Gibson, J. K., Haseler, J.,
595   Hernandez, A., Kelly, G. A., Li, X., Onogi, K., Saarinen, S., Sokka, N., Allan, R. P., Andersson, E., Arpe, K., Balmaseda,
       M. A., Beljaars, A. C. M., van de Berg, L., Bidlot, J., Bormann, N., Caires, S., Chevallier, F., Dethof, A., Dragosavac, M.,
       Fisher, M., Fuentes, M., Hagemann, S., Hólm, E., Hoskins, B. J., Isaksen, L., Janssen, P. A. E. M., Jenne, R., McNally, A.
       P., Mahfouf, J.-F., Morcrette, J.-J., Rayner, N. A., Saunders, R. W., Simon, P., Sterl, A., Trenberth, K. E., Untch, A.,
       Vasiljevic, D., Viterbo, P., and Woollen, J.: The ERA-40 re-analysis, Q. J. Roy. Meteor. Soc., 131, 2961–3012, 2005.

600   Voldoire, A., Sanchez-Gomez, E., Salas y Mélia, D., Decharme, B., Cassou, C., Sénési, S., Valcke, S., Beau, I., Alias, A.,
       Chevallier, M., Déqué, M., Deshayes, J., Douville, H., Fernandez, E., Madec, G., Maisonnave , E., Moine, M.-P., Planton,
       S., Saint-Martin, D., Szopa, S., Tyteca, S., Alkama, R., Belamari, S., Braun, A., Coquart, L., and Chauvin, F.: The CNRM-
       CM5.1   global   climate   model: description   and   basic   evaluation,   Clim.   Dynam.,   40,   2091–2121,
       https://doi.org/10.1007/s00382- 011-1259-y, 2013.

605   Yukimoto, S., Adachi, Y., Hosaka, M., Sakami, T., Yoshimura, H., Hirabara, M., Tanaka, T. Y., Shindo, E., Tsujino, H.,
       Deushi, M., Mizuta, R., Yabu, S., Obata, A., Nakano, H., Ose, T., and Kitoh, A.: A new global climate model of
       Meteorological Research Institute: MRI-CGCM3 – Model description and basic performance, J. Meteorol. Soc. Jpn., 90a,
       23–64, 2012.

Zheng, W. and Yu, Y.: Paleoclimate simulations of the mid-Holocene and Last Glacial Maximum by FGOALS, Advances in
610   Atmospheric Sciences, 30, 684–698, 2013.

Climate
of the Past
Discussions

Table 1. The climate forcing from PMIP3 model output that was used in this study. PMIP3-Ensemble represents the mean of COSMOS, IPSL, MIROC and MPI. The global annual temperature (T) and precipitation (P) difference between LGM and PI is shown for each climate
615   model.

Climate Model	Working Name	Reference	ΔT_{LGM} (K)	ΔP_{LGM} (mm/yr)
CCSM4	CCSM	Brady et al., 2013	4.8	122
CNRM-CM5	CNRM	Voldoire et al., 2013	1.9	70
COSMOS-ASO	COSMOS	Budich et al. 2010	5.3	126
FGOALS-g2	FGOALS	Zheng & Yu, 2013	4.5	109
GISS-E2-R	GISS	Ullman et al., 2014	4.5	102
IPSL-CM5A-LR	IPSL	Dufresne et al., 2013	4.6	146
MIROC-ESM	MIROC	Sueyoshi et al., 2013	4.6	112
MPI-ESM-P	MPI	Jungclaus et al., 2012	4.4	98
MRI-CGCM3	MRI	Yukimoto et al., 2012	4.2	141
PMIP3-Ensemble	PMIP3-Ensemble	-	4.7	120

Figure 1. The North American (red), Greenland (green) and Eurasian (blue) domains used in the ice sheet model. The LGM extent from Abe-Ouchi et al. (2015) is shown in black. This ice sheet reconstruction is used as a boundary condition in the PMIP3 climate model simulations.
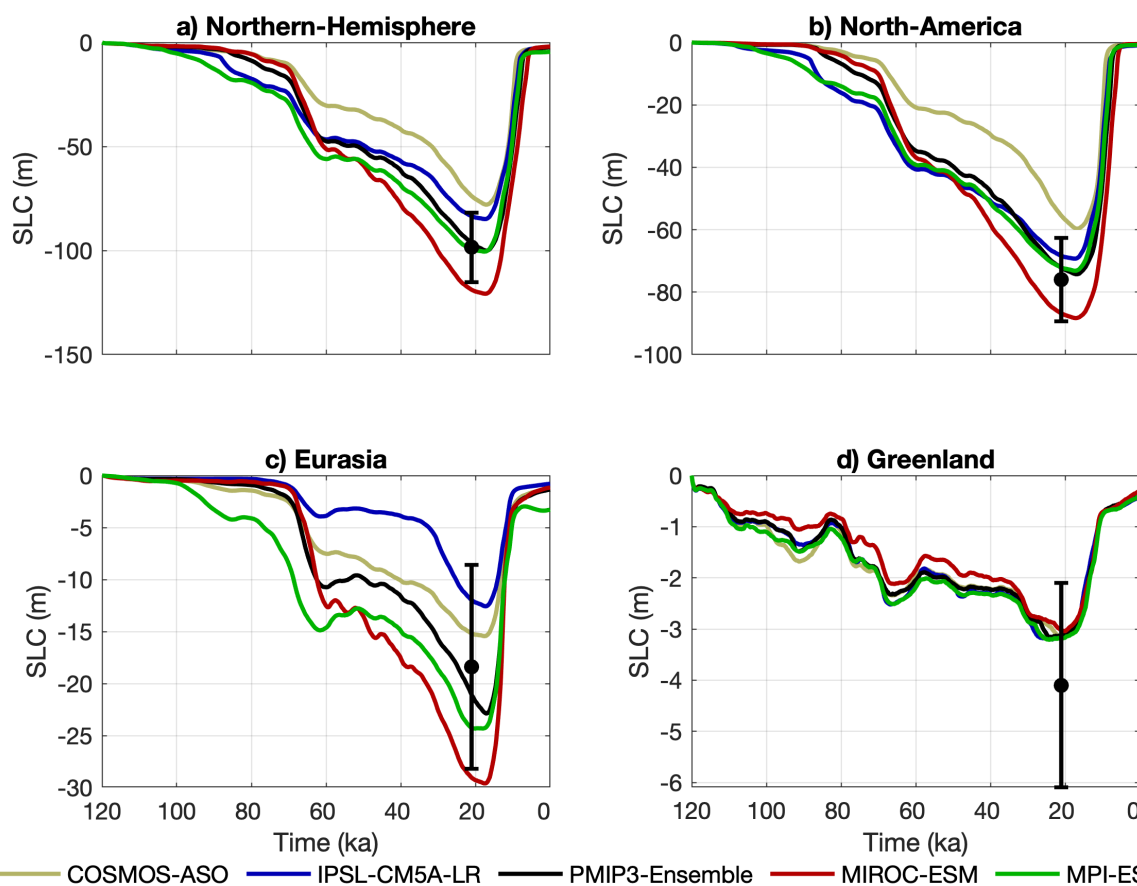
620
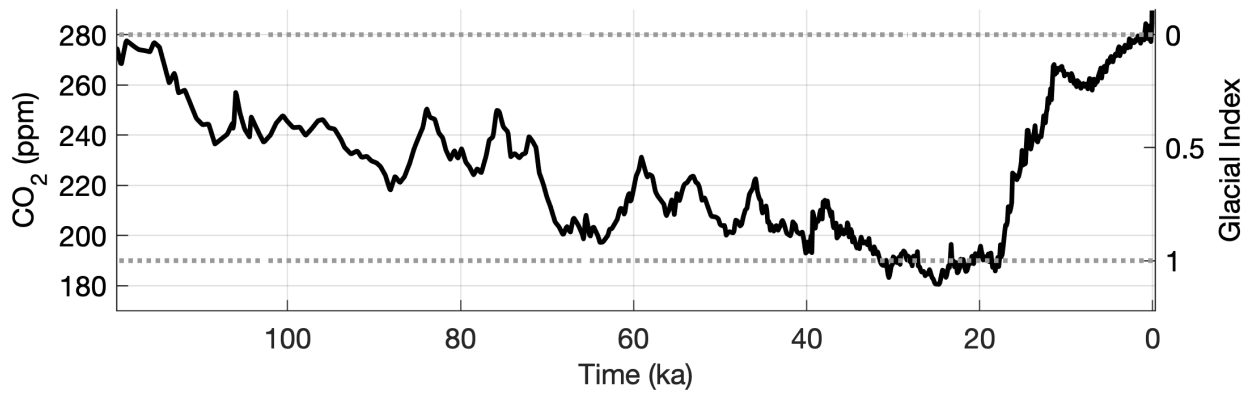
Figure 2. Atmospheric CO_2 concentrations during the LGC from Bereiter et al. (2015) and the corresponding glacial index values. A glacial index value of 1 represents 'full glacial conditions' corresponding to an LGM climate. A glacial index value of 0, or 'full interglacial conditions', represents a PI climate.

625

Climate
of the Past
Discussions

Open Access

EGU

Figure 3. Sea level contribution of the Northern Hemisphere ice sheets using the climate matrix method and the uncertainty range of LGM
ice volume from Simms et al. (2019). Each simulation was forced with a climate obtained from a member of the PMIP3 ensemble.

630
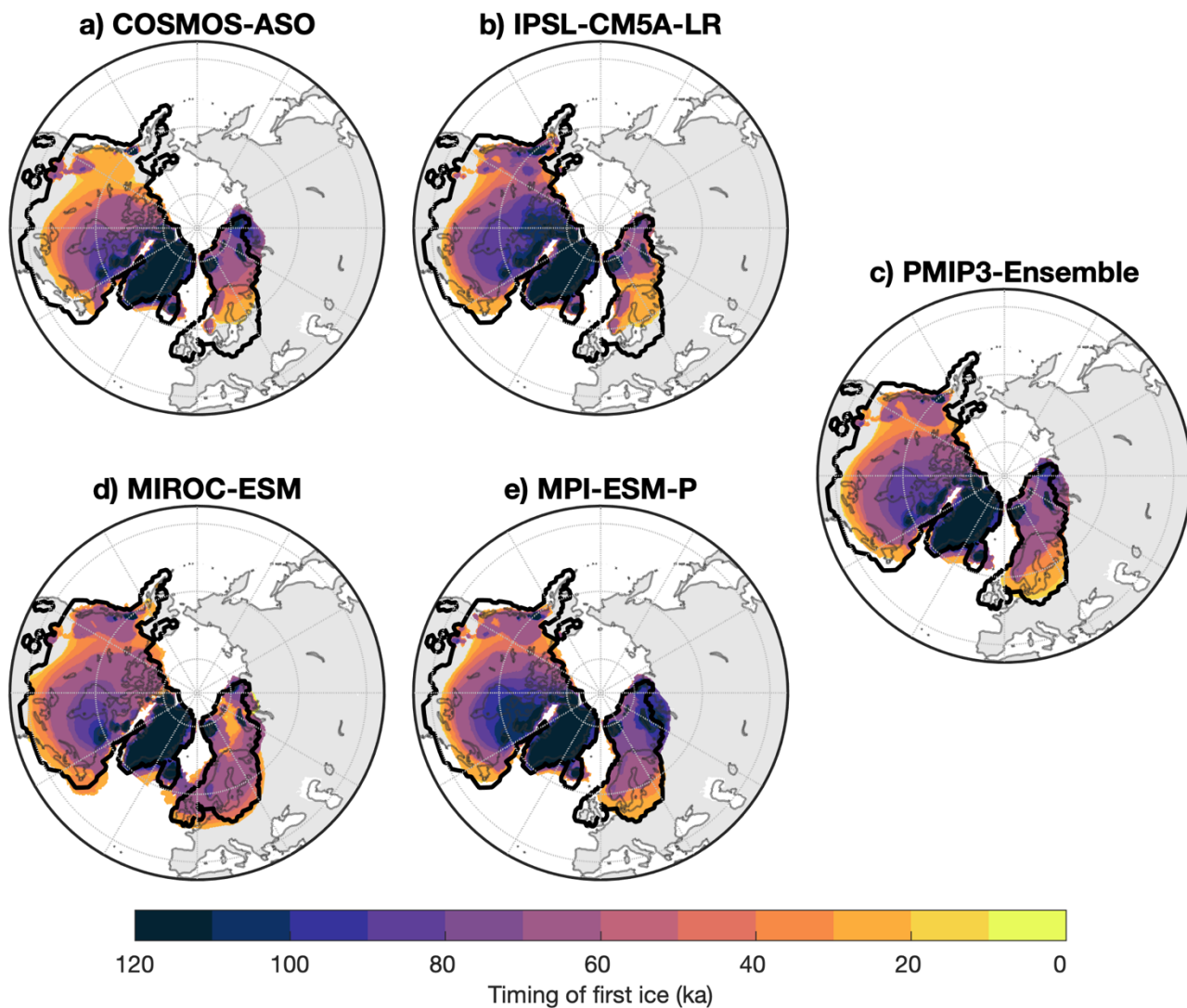
Figure 4. The time at which a region was first covered by ice during the LGC. Darker colours represent earlier inception. Lighter colour regions were covered by ice later. The black contour depicts the ice extent reconstruction Abe-Ouchi et al. (2015) used in the GCM simulations. Each simulation was forced by GCM output from PMIP3 interpolated using the climate matrix method.

Climate
of the Past
Discussions
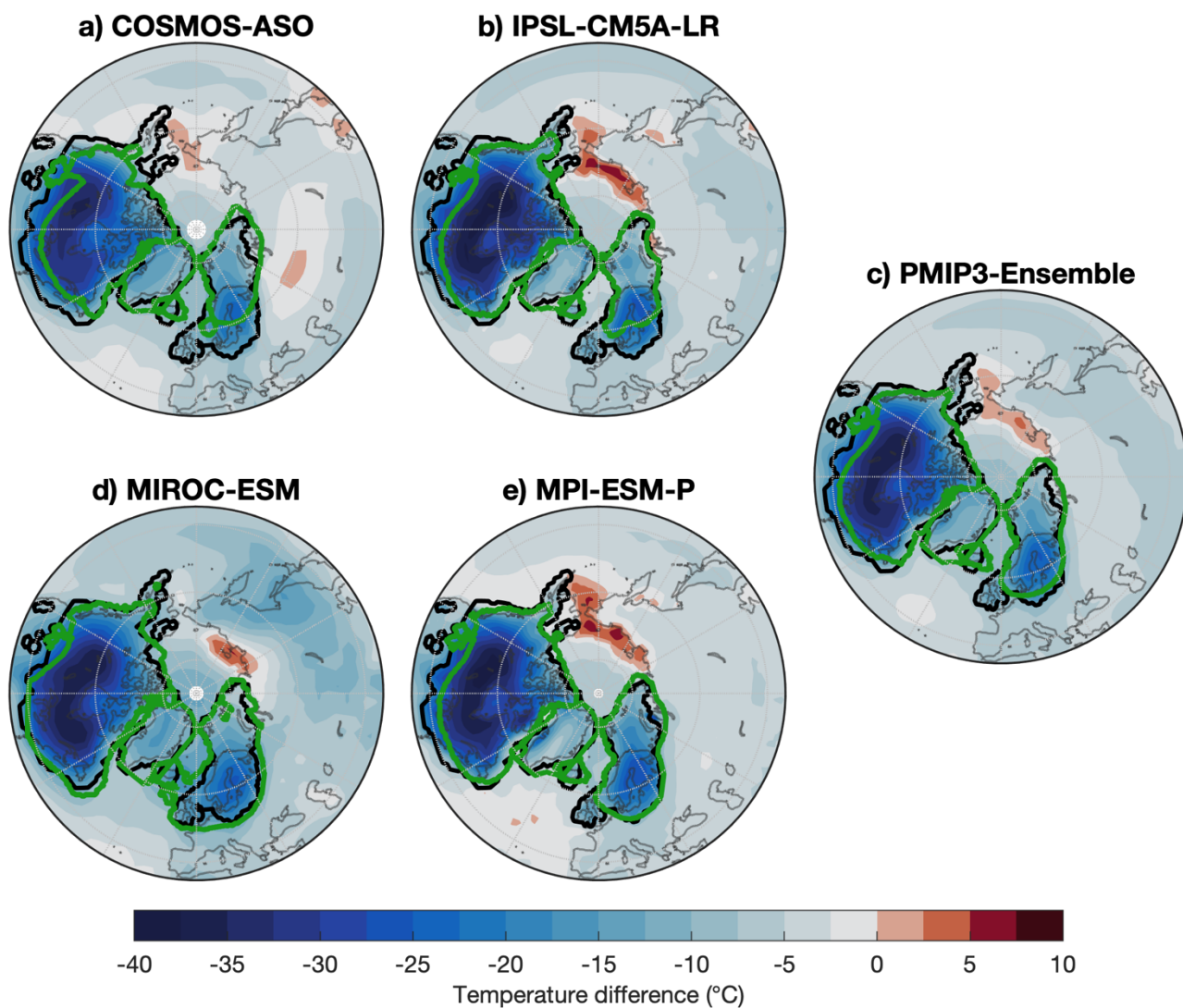
Figure 5. Summer (JJA) temperature differences between LGM and PI. IPSL and MPI have lower temperatures in Arctic Canada compared to the other GCM climates, which results in larger rates of ice growth rate at the onset of the LGC. Black contours represent the LGM extent of the Abe-Ouchi et al., 2015 ice sheets. The LGM extent of the ice sheet model simulations is shown in green.
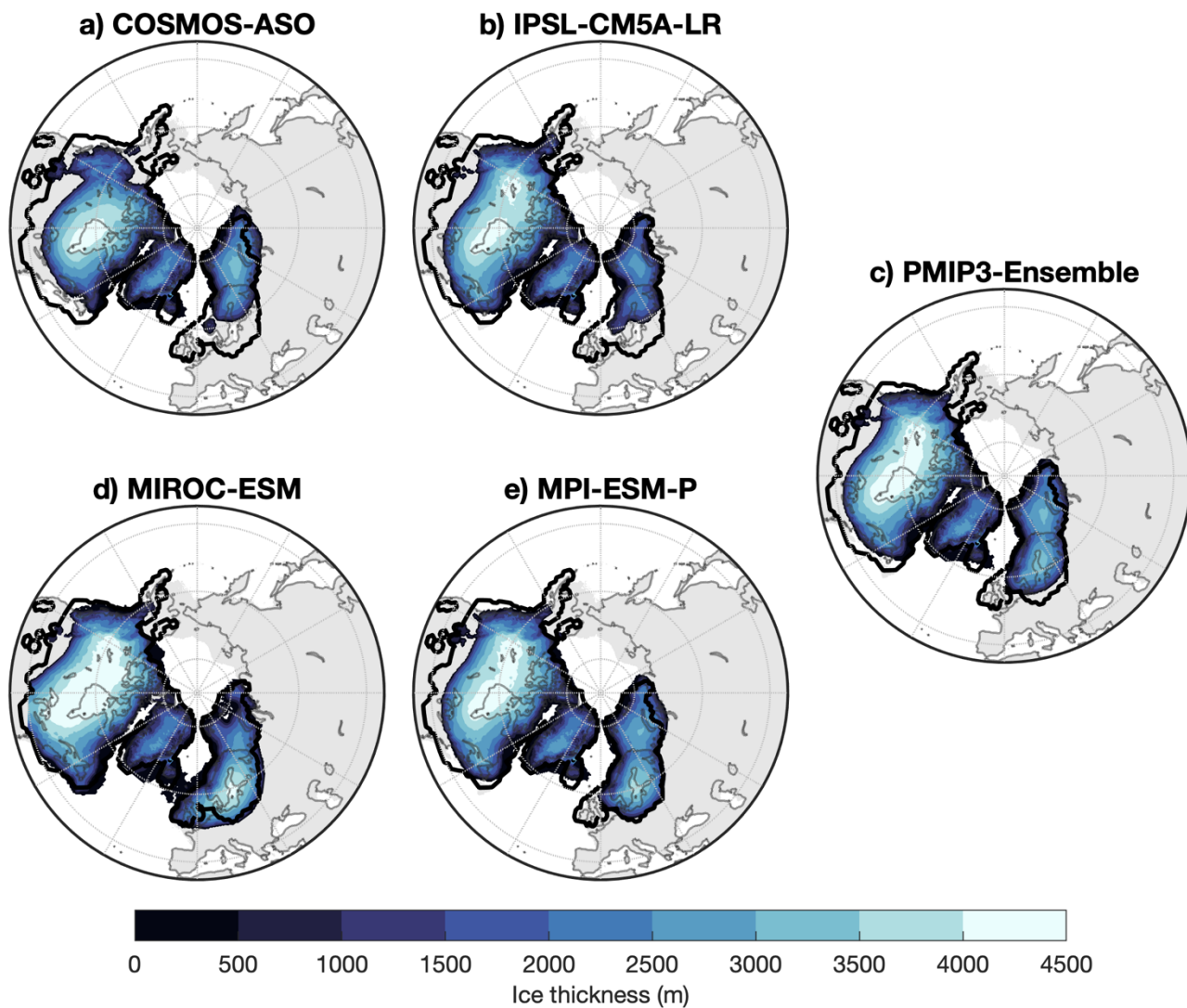
Figure 6. Ice thickness using forcing obtained from members of the PMIP3 ensemble. The ice extent by Abe-Ouchi et al. (2015) is shown
650   as a black contour.
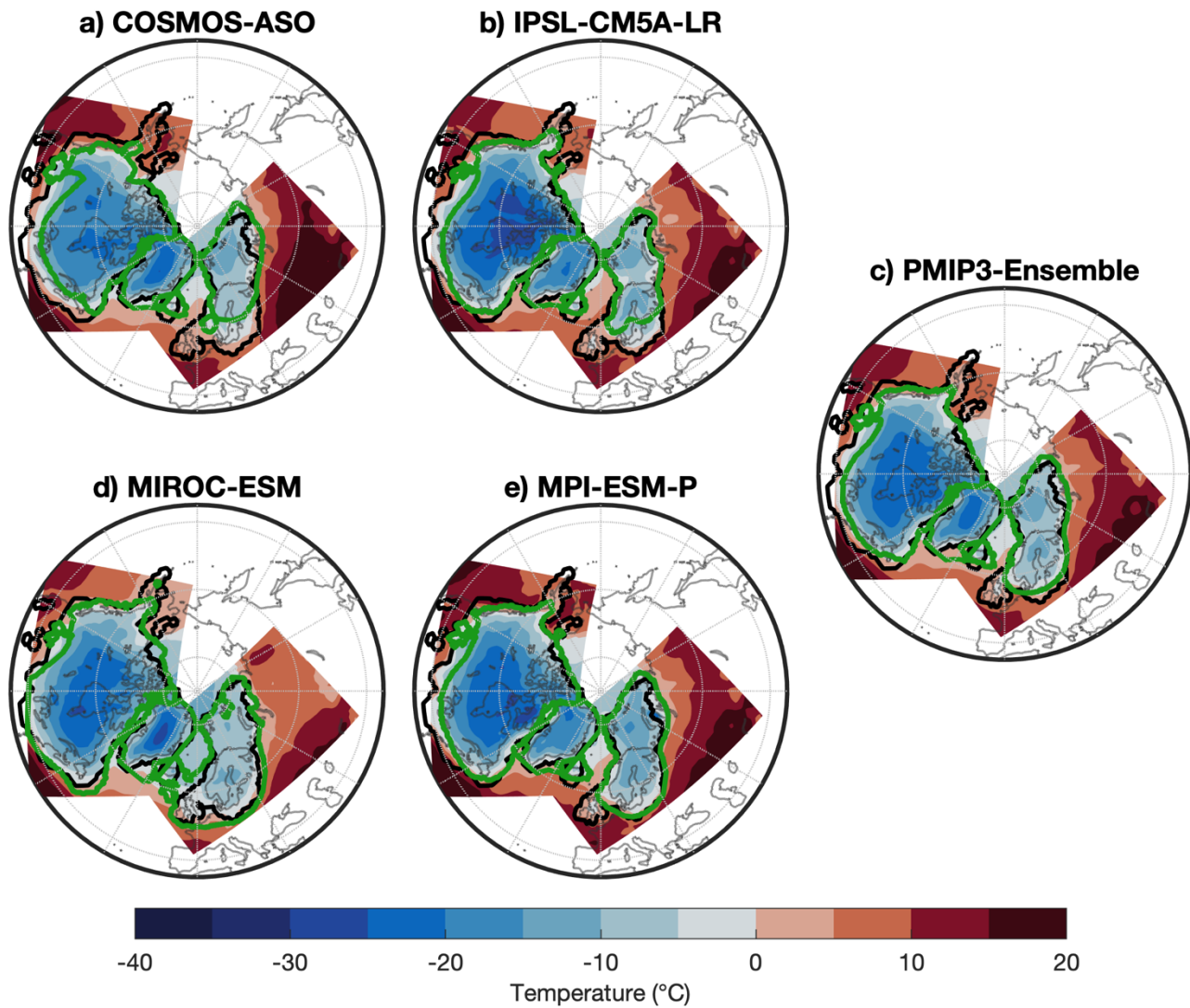
**Figure 7.** LGM summer temperature as it is applied to the ice sheet model. The green contours indicate the extent of the ice sheets that resulted from the GCM forcing. The black contours show the extent of the reconstruction by Abe-Ouchi et al., 2015.
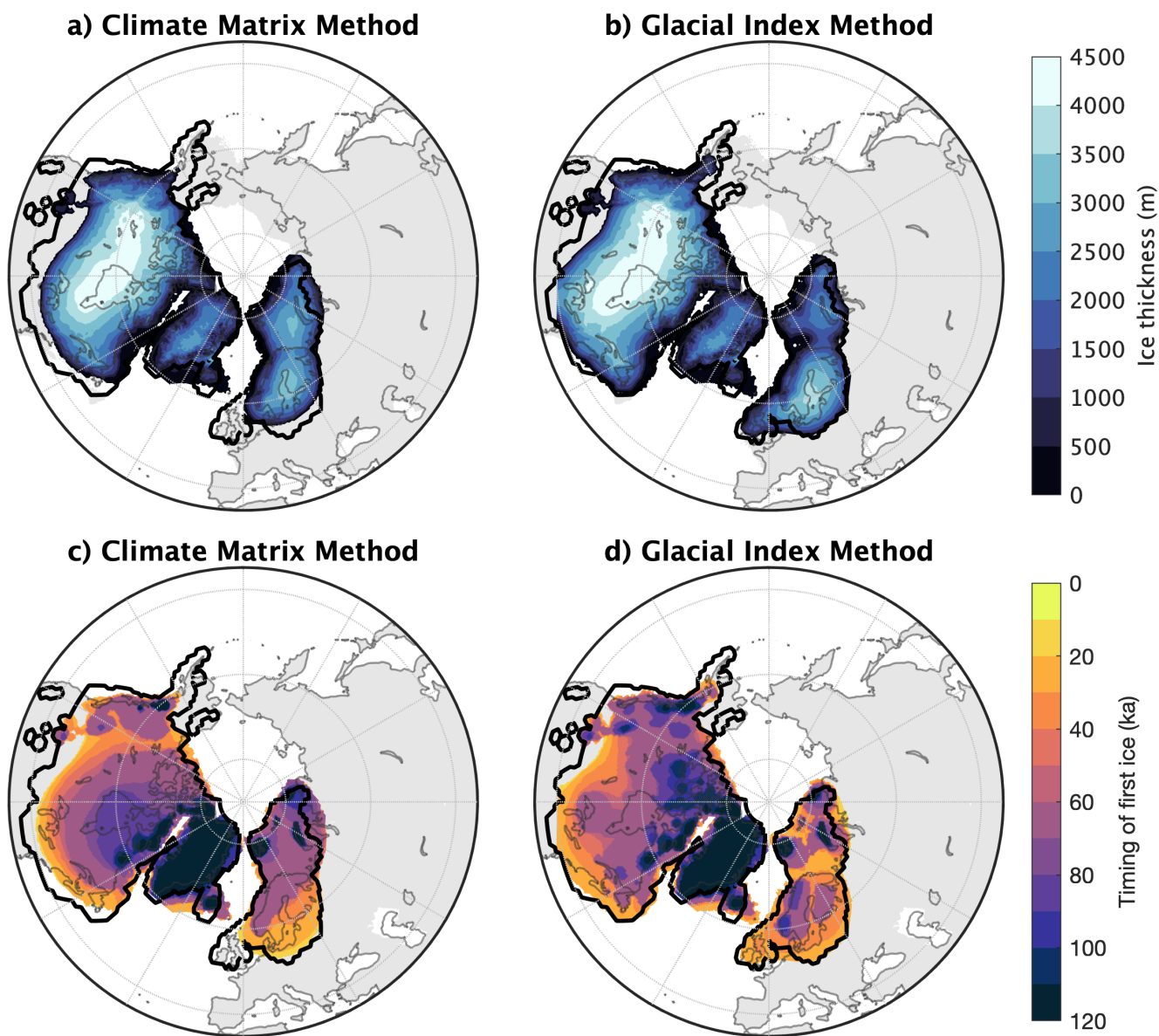
Figure 8. Ice thickness (a,b) and timing of first ice (c,d) of the climate matrix (a,c) and glacial index (b,d) methods. The black contour represents the extent of the ice reconstruction by Abe-Ouchi et al. (2015).

660

31

Climate
of the Past
Discussions
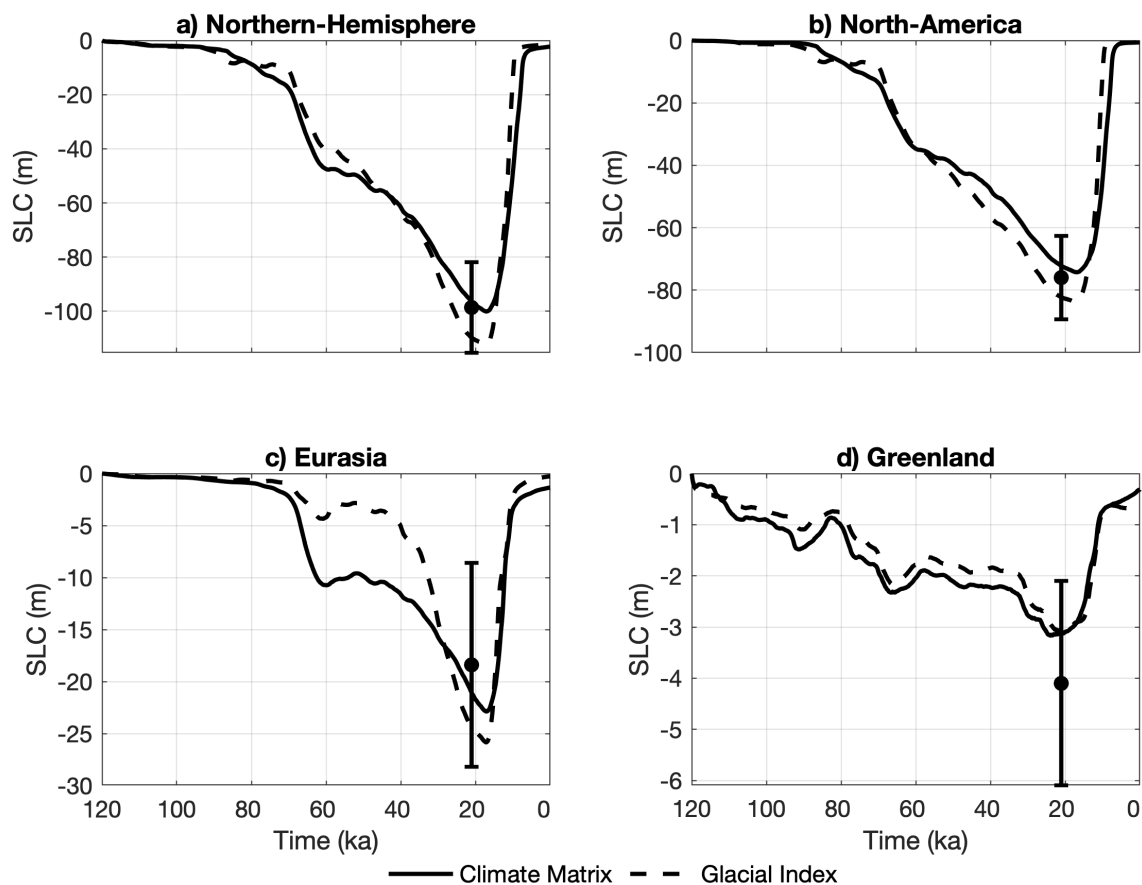
Figure 9. Sea level contribution during the LGC for simulations forced by PMIP3-Ensemble using either the glacial index or climate matrix method.
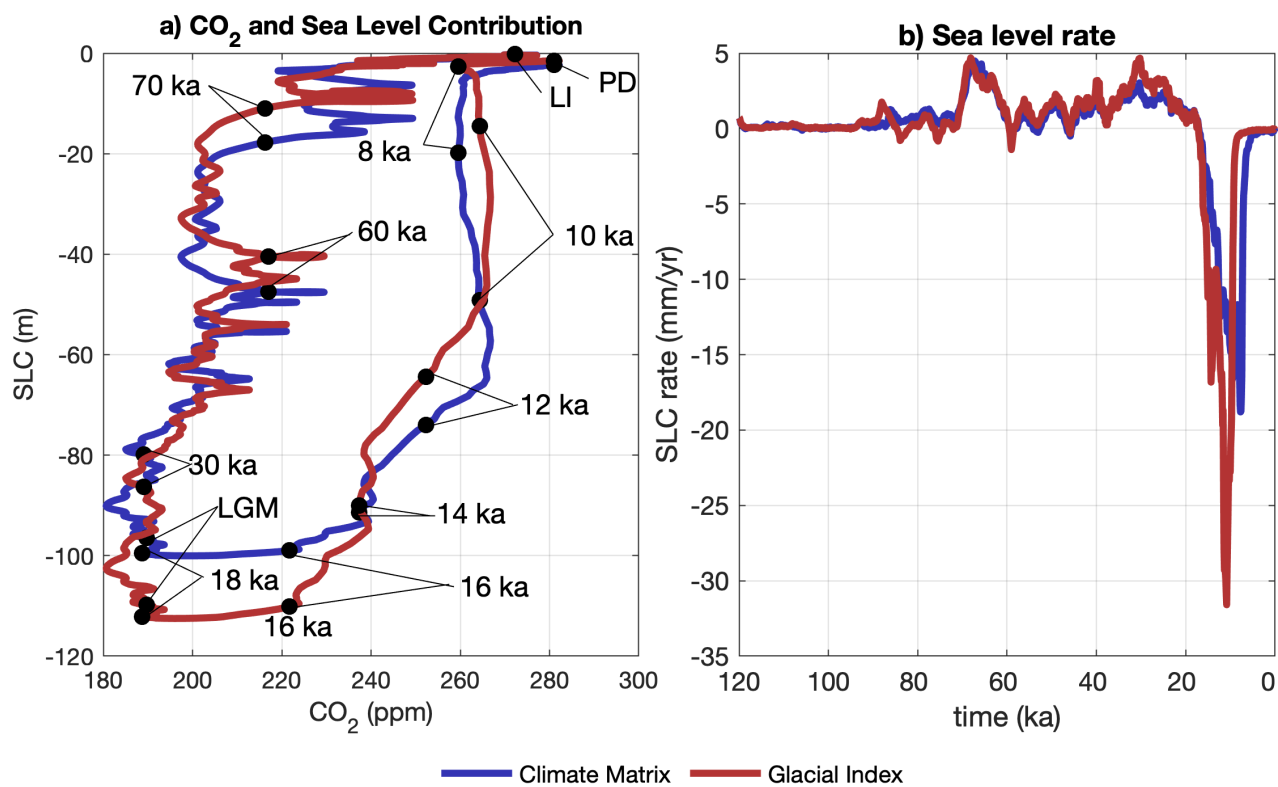
Figure 10. Sea level contribution plotted against CO₂ concentrations (a). And (b), The sea level contribution rate during the LGC.

670